Shear-lag effects in composite glazing panels

Pascual, Carlos; Hartwell, Rebecca; Buskermolen, Pim; Overend, Mauro

DOI
10.1016/j.engstruct.2025.120863

Publication date
2025

Document Version
Final published version

Published in
Engineering Structures

Engineering Structures 342 (2025) 120863

Contents lists available at ScienceDirect

Engineering Structures

journal homepage: www.elsevier.com/locate/engstruct

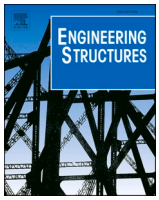

Shear-lag effects in composite glazing panels

Carlos Pascual [a], Rebecca Hartwell [b,*], Pim Buskermolen [b], Mauro Overend [b]

[a] Department of Engineering, University of Cambridge, Trumpington Street, Cambridge CB2 1PZ, United Kingdom
[b] Department of Architectural Engineering & Technology, Delft University of Technology, Julianalaan 134, Delft 2628 BL, The Netherlands

ARTICLE INFO

Keywords:
Adhesive bonding
Composite action
Effective width
Sandwich structure
Shear-lag
Wide flanges

ABSTRACT

Composite glass sandwich panels, consisting of glass face sheets bonded to linear stiffeners (spines) in the core region, can provide significant benefits in material efficiency, reduced thickness, and greater overall transparency. However, current analytical models of their mechanical performance fail to account for the non-uniform longitudinal stress distribution caused by shear-lag effects in wide structural panels. This study redresses this by means of experimental research on composite glazing panels with different loading and geometrical configurations. Six 4-point bending experiments were performed on 34 mm thick, 1000 mm long, and 700 mm wide composite glazing panels, made from soda-lime silica glass face sheets bonded to glass fibre-reinforced polymer core spines. Two types of adhesives were tested: a relatively low stiffness silicone-based adhesive, and a relatively high stiffness epoxy-based adhesive. The shear-lag effects are quantified in terms of effective width ratios (*EWR*). The study showed that the epoxy-bonded panels provided a significant degree of composite action ($DCA = 0.85$) whereas the composite action in the silicone-bonded panels was negligible. Furthermore, it was found that applying the *EWR* values from this study in a recently published analytical model yields predictions of maximum strains at mid-span that deviate by no more than 16 % from the experimental results.

1. Introduction

1.1. Background on composite glazing

Composite glazing panels are mechanically slim (thin) components with a five-layer sandwich configuration: two glass panes (outer face-sheets) sandwiching, and adhesively bonded to, thin frame profiles (inner core) as shown in Fig. 1. These slim components are geometrically classed as panels; the span-to-width ratios of their intended end-applications in the Architecture, Engineering and Construction (AEC) sector typically range between 1 and 3. The out-of-plane flexural response of these panels can range between: (i) the monolithic limit consisting of full composite action between the layers due to shear-rigid interfacial bonding ($G_i \rightarrow \infty$) and; (ii) the layered limit where no composite action is generated between the layers due to frictionless sliding at their interfaces ($G_i \rightarrow 0$) [1]. Recent research demonstrated that a high degree of composite action ($DCA \rightarrow 1$) can be generated between adhesively bonded face-sheets, resulting in a high flexural and buckling resistance [1,2]. This efficient mechanical performance enables the composite glazing panels to span across large openings without any intermediate supporting substructure. It is particularly suitable for building envelope applications (commonly referred to as façades), where conventional insulating glazing units (IGUs) supported by a bulky framing system of mullions and transoms, typically made of steel or aluminium, could be replaced by materially efficient and visually unobtrusive composite glazing panels. Similar applications in other sectors where mass and aesthetics are key requirements could also benefit from such composite glazing panels, for example: vison panels in the automotive sector and display panels in consumer electronics.

1.2. Modelling of composite glazing

The potential benefits of these composite glazing panels are clear, however research on their mechanical performance is scarce. This hinders their development and application in practice. For instance, the strength and stiffness of these multi-layered, multi-material elements are governed by their cross-section, but the associated calculations are not trivial. Euler-Bernoulli simple beam theory does not adequately represent the mechanical response because the partial effectiveness of the full cross-section is not accounted for, particularly shear deformations caused by *shear-lag effects* in both (i) the through-thickness (in the adhesive layers) and (ii) the in-plane (across the width of the glass face-

* Corresponding author.
E-mail address: contact@rebeccahartwell.com (R. Hartwell).

https://doi.org/10.1016/j.engstruct.2025.120863
Received 24 March 2025; Received in revised form 13 June 2025; Accepted 22 June 2025
Available online 8 July 2025

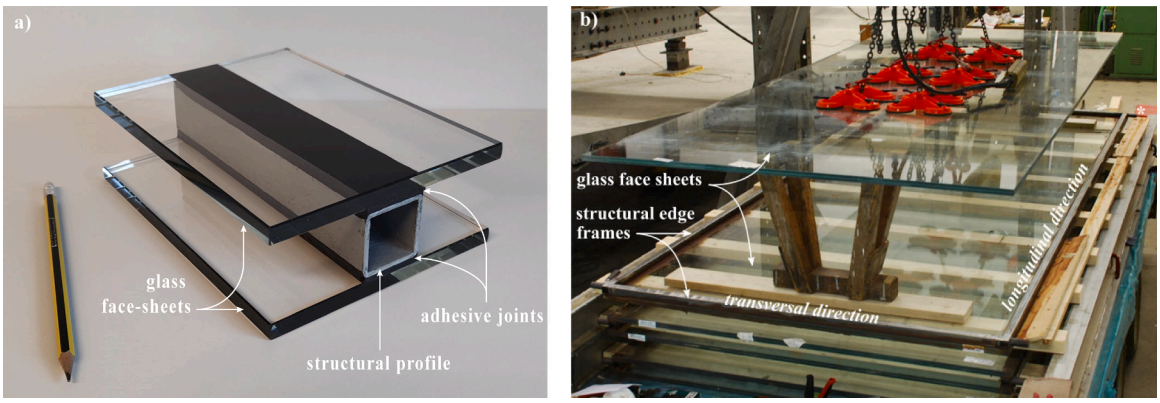

Fig. 1. Five-layer (glass-adhesive-spine-adhesive-glass) composite glazing panel prototypes of a) small-scale (mock-up) dimensions and central profile (spine) b) assembly stage of large-scale panels with edge-frame (perimeter) spines showing upper face sheet supported by temporary timber props prior to applying adhesive, as published in previous work [1].

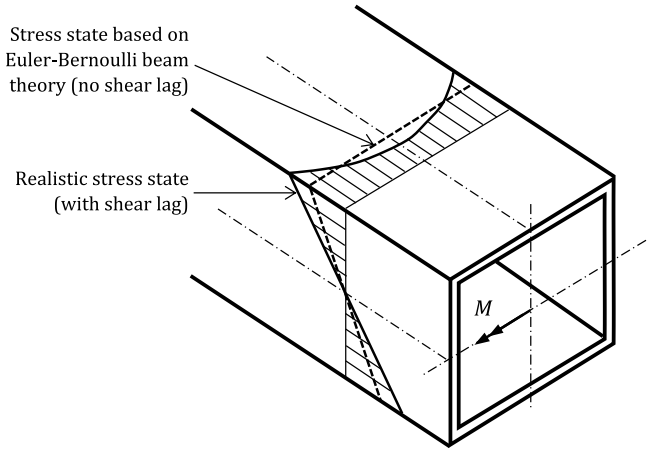

Fig. 2. Shear-lag effects in thin-walled steel hollow section (schematic).

sheets) directions are neglected. The former has been recently analysed and modelled in previous research on narrow multi-layer panels [3–5], whilst the latter, which is particularly pronounced in the specific case of wide composite glazing panels, has yet to be quantified and is therefore the object of the present study. Models such as that by *Heiniuso and Pajunen* and *Chen et al.* neglect shear deformations in the frame profile and therefore cannot be readily applied to composite glazing configurations [3,4]. The model presented by *Pascual et al.* considers the composite glazing panel as a beam of multiple layers with non-uniform widths and assumes linear elastic materials [5]. The model accounts for bending and shear deformations along the local and global centroidal axes in the through-thickness plane of the composite panel. The geometrical compatibility between these deformations depends on the mechanical parameter a^2, given by Eq. [1]:

$$a^2 = \frac{U}{D_{local} \bullet \left(1 - \frac{D_{local}}{D_{global}}\right)} \tag{1}$$

where U, is the shear stiffness of the composite glazing panel, and D_{local}, and D_{global}, are the local and global flexural rigidities, respectively. These parameters depend solely on geometric and material properties. Further information on how to calculate these parameters and on the analytical solutions for strains and deflections, are given by *Pascual et al.* [5]. The present study extends this recent work by investigating the applicability of this model (originally developed for narrow multi-layer beams) to wide multi-layer panels by using an appropriately reduced (effective) width for determining the flexural rigidities and shear stiffness to account for shear-lag effects. Shear-lag effects shown in Fig. 2 are well-documented in thin-walled steel cross-sections subjected to flexure (e.g. plate girders and box girders), in which a shear flow develops between the web elements (spine cores) and the flange elements (face-sheets) of a thin-walled steel structure [6,7]. This causes in-plane shear distortion of the flange plate with longitudinal strain (and corresponding stress) in the flange plate decaying from a maximum near the web to a minimum at the furthest distance from the web. Thus, the axial deformations in the flange regions away from the web "lag behind" the regions close to the web [8]. The shear-lag phenomenon results in reductions of the effective flexural strength and stiffness of a cross-section, which in structural engineering practice is often expressed as the effective width ratio (*EWR,* also referred to as effective breadth ratio), i.e. the ratio between the statically equivalent width (i.e. with no decay of axial stress) and the actual physical width.

Closed form analytical solutions exist for capturing this phenomenon for mono-material cross-sections. In particular, *Reissner* provided a mathematical derivation for the reduced strength and stiffness at a given cross-section, showing that longitudinal strains and stresses in the flanges decay parabolically with increasing distance from the web [9,10]. This research forms the basis of the subsequent work on shear lag and *EWR* leading to the more recent analytical methods developed by *Yossef and Chen* for shear-lag effects in bi-material (three-layer) sandwich panels [11,12]. *Yossef and Chen* showed that the *EWR* increases with increasing span-to-width ratio and increases with decreasing *DCA* [11,12]. They also showed that using the same *EWR* for a range of *DCA*s leads to an error in the prediction of mid-span stresses of up to 36 %.

1.3. Study objectives

There is no known analytical solution for predicting the shear-lag effects in five-layer composite configuration used in composite glazing panels (Fig. 1). However, recent experimental work on composite glazing indicates that shear-lag effects are significant. For example, the experimental work by *Pascual et al.* provided initial evidence on *EWR* ≈ 0.60 for *DCA* > 0.90 in panels with span-to-width ratio ≈ 2 [1]. Additionally, substituting an effective (reduced) width for the real width into the model of *Pascual et al.* yielded an accurate prediction of deflections [1,5]. However, to-date, no direct empirical data exists on the shear-lag effects in composite glazing panels. The present paper seeks to redress this by means of experimental investigations on five-layer

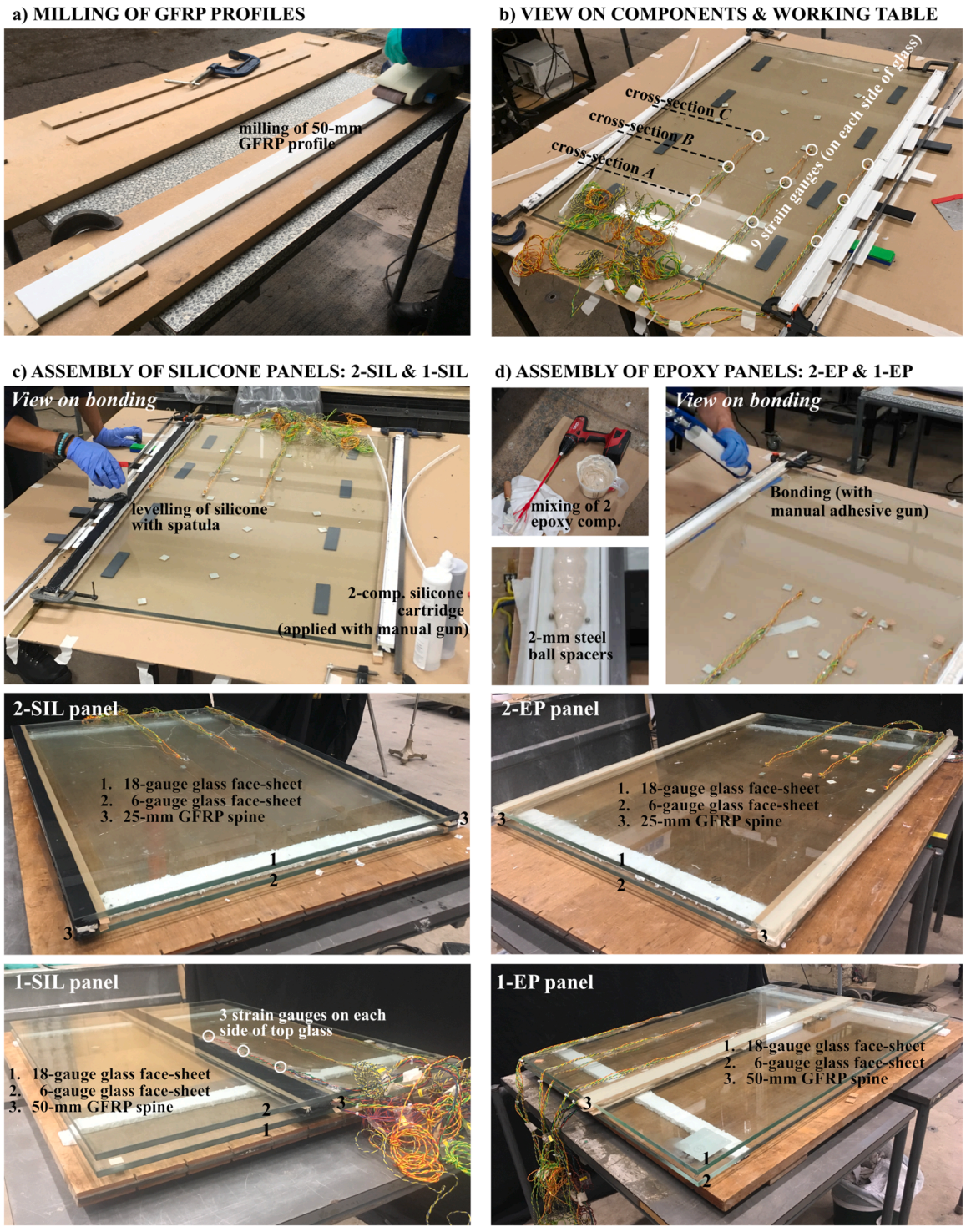

Fig. 3. Fabrication of the four composite glazing panels, including a) milling of GFRP spines, b) view on the assembly working table, c) assembly of silicone panels 2-SIL and 1-SIL bonded with black silicone Dow 121 and d) assembly of epoxy panels 2-EP and 1-EP bonded with white epoxy Körapox EP40619.

Table 1
Four composite glazing panels and six experimental loadings (4-point bending set-up).

Panel	10-mm thick GFRP spine		2-mm thick adhesive		Experimental loading (totalling *2 P*) on top face-sheet			
Label	**Type**	**Width (mm)**	**Type**	**Width (mm)**	**Load over cavity (config. *Cav*)**	**Load on spine (config. *Sp*)**	**Load max. (kN)**	**Exp. n°**
Silicone panels:								
2-Sil*	Double	25 + 25	Silicone	25 + 25	2•*(P)*	-	$2{\cdot}P = 3$*	1
2-Sil	Double	25 + 25	Silicone	25 + 25	-	4•*(P/2)*	$2{\cdot}P = 11$	2
1-Sil	Single	50	Silicone	50	-	2•*(P)*	$2{\cdot}P = 21$	3
Epoxy panels:								
2-Ep*	Double	25 + 25	Epoxy	25 + 25	2•*(P)*	-	$2{\cdot}P = 3$*	4
2-Ep	Double	25 + 25	Epoxy	25 + 25	-	4•*(P/2)*	$2{\cdot}P = 17$	5
1-Ep	Single	50	Epoxy	50	-	2•*(P)*	$2{\cdot}P = 24$	6

*Non-destructive experiments (cavity loading configuration)

Table 2
Material properties of composite glazing panels.

Material	Law σ - ε	E (MPa)	ν (-)	G (MPa)
Glass	Linear	70000	0.23	28455
GFRP	Linear	28000	0.30	3000
Epoxy	Linear	380	0.39	137
Silicone	Linear	1.5	0.49	0.50

composite glazing panels with monolithic face-sheets and varying degrees of composite action. It investigates the relationship between the degree of composite action (*DCA*) and the effective width ratio (*EWR*).

This paper first describes the fabrication, instrumentation, and 4-point bending test set-up of 4 composite sandwich panels each with different configurations of edge/central core spines and compliant/stiff adhesives. The panels and the test set-up constitute the first of their kind experimental tests on shear-lag effects in composite glazing. This is followed in Section 3 by a description of the observations and experimental results from these novel tests. The results are analysed and discussed in Section 4 where the deflections (measured using displacement transducers) and strain distribution (measured using strain gauges) are analysed to determine the new *EWR* and *DCA* values. The existing analytical model for multi-layer beams by *Pascual et al.* is populated with the new *EWR* values obtained from the present study to assess its accuracy in predicting maximum strains and deflections [5]. Finally, a summary of the findings and recommendations for future research is listed in Section 5.

2. Experimental procedure

Four composite glazing panels (1000-mm long and 700-mm wide) were fabricated in a sandwich configuration: outer glass face-sheets adhesively bonded to inner spine cores. Two sets of panels, namely single-spine and double-spine panels, were assembled with 1000 mm long spines positioned along the centroidal axis and lateral edges, respectively, as shown in Fig. 3. Each set was composed of 2 panels, one bonded with an epoxy adhesive and one bonded with a silicone adhesive. The panels were labelled according to the number of spines and type of adhesive, e.g. 1-Ep & 2-Ep refer to the single (central)-spine & double (edge)-spine panels bonded with epoxy (Ep), see Table 1.

2.1. Materials and geometry of panels

The reinforcing spines consisted of 10-mm thick glass fibre-reinforced polymer (GFRP) pultruded profiles manufactured by Fiberline Composites according to *EN 13706–3:2002* [13]. The spines were 50 mm wide (for single spine panels) and 25 mm wide (for double spine panels). All spines were 1000 mm long. The face sheets of all panels were made of 10 mm thick monolithic fully toughened soda-lime-silica float glass (panel dimensions 1000 × 700 mm) manufactured by Interpane according to *EN 572–2:2012* [14] and subsequently heat-treated in accordance with *EN 12150–2:2004* [15]. The overall dimensions of the panels were selected by scaling down (by a factor of 3, approximately) the size of a standard composite glazing panel for façade application based on previous research [1]. A sufficient bond width (25 mm) was required to effectively clamp the edge of the glass face-sheets to each lateral spine appropriately, a double width (50 mm) was required for the central spine [1]. The spines and face sheets were bonded with either a two-component epoxy Körapox EP40619 (epoxy-panels) or a two-component silicone Dow 121 (silicone-panels) manufactured by H. B. Fuller-Koemmerling and Dow, respectively. All adhesive bond line thicknesses were 2-mm. This thickness complied with manufacturer recommendations. The selection of the adhesive and frame material was based on a wide range of criteria related to their mechanical performance [1,2,5,16–18] and intended to produce high and low degrees of composite action (*DCA*) for the epoxy-and silicone-bonded panels, respectively. Silicone adhesive was chosen as representative of structural silicones (extensively used in the AEC industry) with the intent to demonstrate their lower bound performance in terms of *DCA*.

The elastic modulus (E), shear modulus (G) and Poisson's ratio (ν) of all materials are shown in Table 2 and are determined as follows. For (orthotropic) GFRP spines, the relevant values for E (in pultrusion-direction), and for G and ν (in the pultrusion-direction planes) were obtained from the manufacturer datasheets. Properties in other directions were not relevant as the spines were only bending in the (axial) pultrusion direction [19]. For (isotropic) glass, the reported elastic properties are standard values for commercially produced glass [20,21]. For (isotropic) adhesives, the Poisson's ratios were obtained from (i) *Pascual and Overend* for epoxy [2] and (ii) *Larson* for silicone [22]. Elastic moduli were approximated from hardness data using a formula by *Qi et al.* for epoxy (75 shore D) [23], and a formula by *Ruess* for silicone (35 shore A) and reported by *Larson* [22]. Shear moduli were deduced from linear elasticity. A comparison between elastic properties approximated from hardness data and from experimental lap-shear testing is shown in Appendix A.

Following from previous research, maximum adhesion was achieved by removing the outer layer of the GFRP spines prior to bonding [2]. Therefore, prior to the assembly of all panels, GFRP surfaces were milled down by approximately 0.1-mm using an electric-powered sanding device to remove the resin-rich surface layer of the GFRP as shown in Fig. 3a. Subsequently, all glass surfaces were cleaned with acetone. The width and thickness of the adhesive joint were controlled by means of Teflon masking tape and 2mm-diameter steel spherical spacers, respectively (see Fig. 3). Preparation and assembly of the panels was performed in laboratory conditions at 23 ± 2°C and a relative humidity of 50 ± 5 %. The assembled panels were stored in these conditions for a

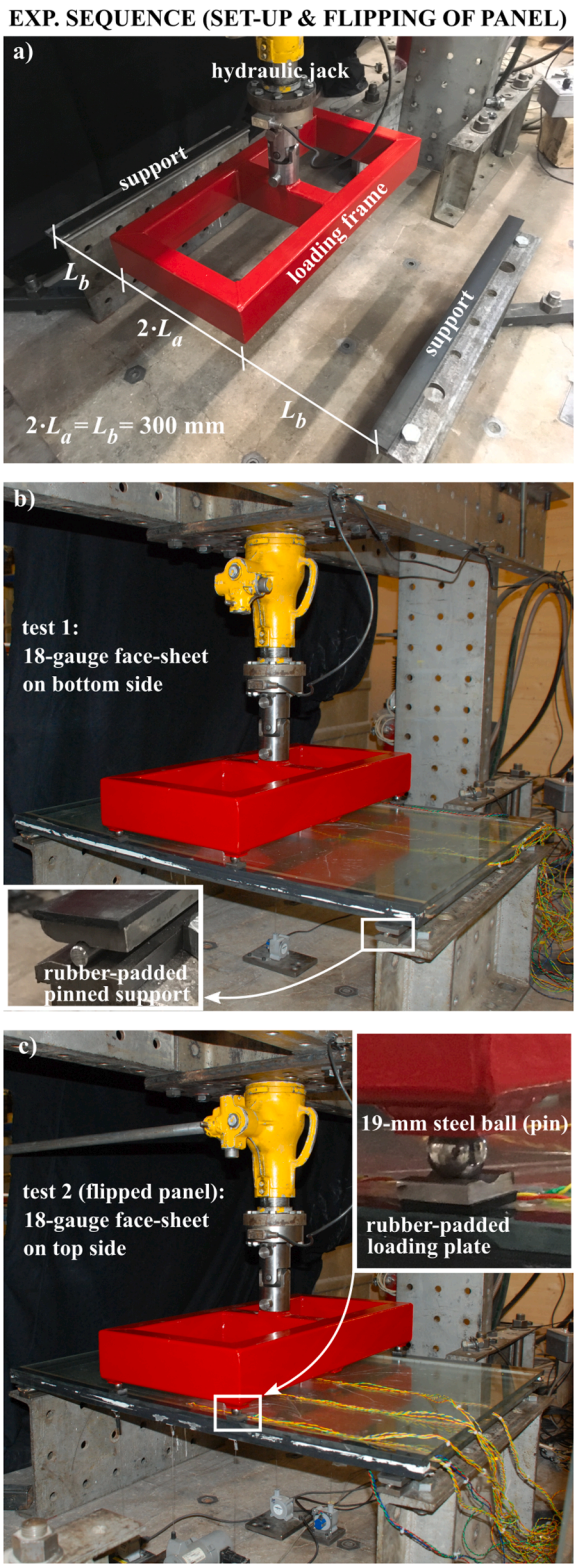

Fig. 4. Test sequence for one (out of six) representative experiments: a) loading set-up, b) first test with fully monitored face-sheet in bottom position, and c) second test with fully monitored face-sheet in top position.

minimum of 50 days prior to testing.

2.2. Experimental set-up

Six experiments were performed on the four fabricated panels. The panels were tested in a 4-point bending configuration using the stiff reaction frame set-up shown in Fig. 4. The patch loads, totalling $2{\cdot}P$, were applied using a stroke-controlled hydraulic jack fitted with a 50 kN load cell and introduced at approximately 1 mm•min^{-1} (mid-span deflection) – sufficiently slow to produce low strain-rates and dissipate viscous effects in the polymeric materials. The patch loads were applied to the outermost surface of the top glass face-sheet by means of rotationally-free rubber-padded steel plates (25 × 25 × 5 mm). The outermost surface of the bottom face-sheet was supported at opposite ends, along the 700 mm width, on rotationally free rubber-padded pinned steel plates (740 × 40 × 10 mm). The total span (L = 900 mm), load span ($2L_a$ = 300 mm) and shear span (L_b = 300 mm) were the same in all experiments as shown in Fig. 5 and Table 3.

The six experiments were performed at 23 ± 2°C and a relative humidity of 50 ± 5 %. The vertical deflections of the bottom face-sheet were measured at the centre and lateral edges (both at mid-span and loaded cross-sections) using four compact string pot wire transducers (Fig. 5a). Two additional wire transducers, not represented in Fig. 5a, also attached to the bottom face-sheet were used to verify the double symmetry of deflections with respect to the two symmetry axes of the panel. Additionally, eighteen strain gauges were bonded on one quadrant of one glass face-sheet: nine on the outer surface and nine on the inner surface (Fig. 5a). Finally, six strain gauges were bonded on one quadrant of the opposite glass face-sheet: three on the outer surface and three on the inner surface. Each experiment comprised two bending tests. The position of the fully monitored face-sheet was flipped in one of the tests: in the bottom position first, and the top position second, see Fig. 4. Full strain data maps of the glass face-sheets were obtained this way.

The six experiments permitted the investigation of two load configurations, (see Fig. 5 and Table 1): *a*) cavity loading referred to as config. *Cav*, on 2-Ep and 2-Sil panels (i.e. two experiments) and *b*) spine loading referred to as config. *Sp*, on 2-Ep and 2-Sil (i.e. two experiments) and on 1-Ep and 1-Sil panels (i.e. two experiments). In config. *Cav,* the loads were applied on the glass over the cavity (with two patch loads aligned with the centroidal axis), and in config. *Sp,* the loads were applied on the glass over the spines (with two and four patch loads aligned vertically above the spines, for single and double spine panels, respectively). For each panel, two non-destructive config. *Cav* tests were performed, followed by one non-destructive config. *Sp* test, and finally a config. *Sp* test performed to failure. Every non-destructive test was performed up to $2{\cdot}P$= 3 kN. This made it possible to combine data from the first (non-destructive) and second (destructive) tests to assemble strain data maps of both face-sheets – the data from the six-gauge quadrant was used to verify the merged data from both tests.

Even distribution of loads was ensured by articulated connections between the loading frame and the hydraulic jack through the use of a 1-axis (simple) and 2-axis (universal) joint, for two- and four-patch experiments, respectively. The sensor positions and the loading of panels are shown in Fig. 5. All sensors (displacement transducers, strain gauges and load-cell) were calibrated prior to testing and special care was taken to ensure symmetric loading.

3. Experimental observations and results

3.1. Load-deflection responses and DCA

The top (compression) glass face sheet fractured first for the single-spine epoxy panel (1-Ep) and double-spine silicone panel (2-Sil) whereas in the other panels (2-Ep and 1-Sil) both face sheets fractured simultaneously. In cases where a face sheet remained unfractured, the loading was increased linearly until the second glass pane fractured. All fractures were highly explosive (due to the release of energy of fully toughened glass) preventing a clear identification of crack initiation.

The tests to failure (config. *Sp*) show that double-spine panels fractured prematurely compared to single-spine panels. This was attributed

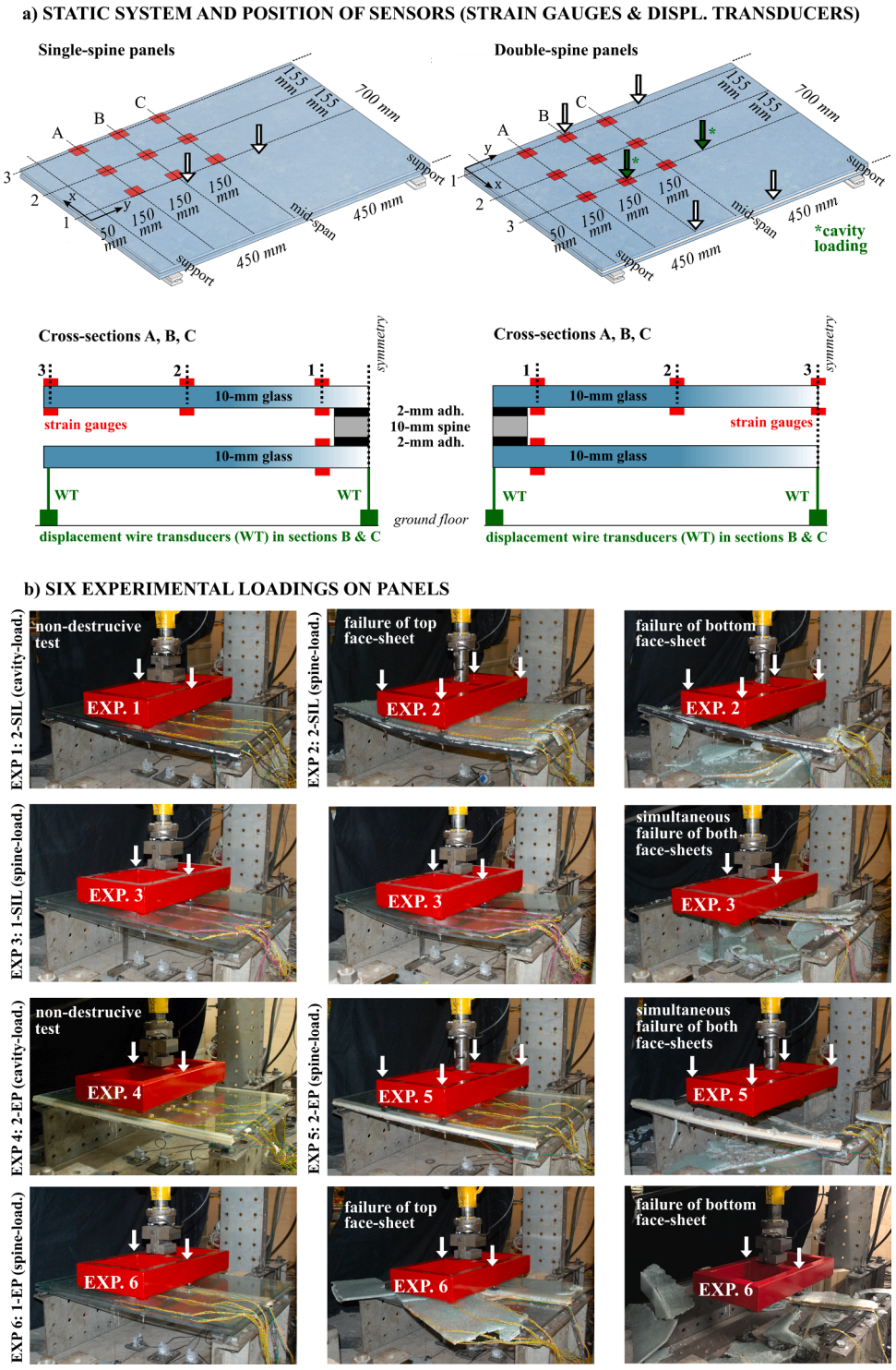

Fig. 5. Views of a) static system, position of sensors and cross-sections, and b) experimental loading of composite glazing panels. Note: arrows indicate position of loading, and images correspond to the second test of every experiment (i.e. top face-sheets equipped with 18 strain gauges).

Table 3
Geometry and modelled mechanical properties. The average *EWR* values are obtained from experimental data reported in Section 3. Global and local flexural rigidities and shear stiffness are defined in *Pascual et al.* and reported in Section 1 [5].

Panel	Load location & Geometry					Modelled mechanical properties			
Label	Loc.	L (mm)	L_a (mm)	L_b (mm)	W (mm)	EWR (-)	D_{global} ($\bullet 10^{11}$ N$\bullet$mm^2)	D_{local} ($\bullet 10^{9}$ N$\bullet$mm^2)	U ($\bullet 10^{3}$ N)
Silicone panels									
2-Sil*	Cav.	900	150	300	700	0.920	1.375	7.630	3.321
2-Sil	Sp.	900	150	300	700	0.867	1.296	7.198	3.321
1-Sil	Sp.	900	150	300	700	0.911	1.364	7.572	3.321
Epoxy panels									
2-Ep*	Cav.	900	150	300	700	0.673	1.023	5.705	826.8
2-Ep	Sp.	900	150	300	700	0.739	1.104	6.148	826.8
1-Ep	Sp.	900	150	300	700	0.631	0.944	5.273	826.8

* Non-destructive experiments (cavity loading configuration)

to the lower edge strength of glass, which in the case of the double spine panels are in a state of high tensile stress [24,25]. However, post-fracture analysis is outside the scope of this study on shear-lag effects and will not be discussed further in this paper.

The load *vs.* mid-span deflection (at the centre of the bottom face-sheet) is shown up to fracture in Fig. 6a (config. *Sp*) and in further detail at lower loads in Fig. 6b (Ep-panels, config. *Cav & Sp*) and Fig. 6c (Sil-panels, config. *Cav & Sp*). Figs. 6b and 6c also highlight the theoretical layered and monolithic limits indicating zero composite action ($DCA = 0$) and full composite action ($DCA = 1$), respectively. A single representative value of DCA_w of every panel is shown in Figs. 6b and 6c based on their mid-span deflection w. In contrast, in the following Section 3.2, detailed values of DCA_ε (across the width and span) are calculated based on strains. The single representative DCA_w, is calculated by direct proportionality across the range of deflections as proposed by *Pascual et al.* [5]:

$$DCA_w = \frac{w_{DCA=0} - w}{w_{DCA=0} - w_{DCA=1}} \times 100\% \quad (2)$$

where mid-span deflections for layered ($w_{DCA=0}$) and monolithic ($w_{DCA=1}$) behaviour are calculated analytically with the model governed by Eq. [1] and detailed by *Pascual et al.* [5], and w, is the experimental mid-span deflection of the tested panel. The silicone panels exhibited a similar stiffness in all experiments, particularly during unloading, and approximately followed the layered limit response ($DCA_w \approx 0$). The epoxy panels exhibited much stiffer responses ($DCA_w \approx 0.85$) and were closer to the monolithic limit. In each test the responses were linear up to first fracture.

3.2. Strain and DCA maps

Normalised longitudinal (in the direction of the span) strain maps in glass face-sheets (at a load $2{\cdot}P = 2$ kN) are shown in Fig. 7 for the six bending experiments. The strain results were mirrored twice in-plane (owing to the double symmetry of geometry and loading) to obtain full strains maps on the glass surfaces. The location of the strain gauges is indicated with outlined rectangles. Strains are plotted in rectangular cells, i.e. in a Voronoi-like fashion, so that the border between cells lies halfway between the corresponding gauges. Normalised strains are plotted for each experiment in a 0–100 % scale – the maximum measured strain (in absolute terms) set both the upper (tension in red) and lower (compression in blue) limits of the scale, see Fig. 7. White regions refer to cells with normalised strains of 0%. Grey hatched regions correspond to areas where no reliable data was recorded due to dysfunctional gauges. Data from dysfunctional gauges was excluded from the calculations of *EWR*.

The strain distribution maps show three notable phenomena along the three Cartesian directions. Firstly, in through-thickness-direction: the innermost (i.e. core-facing) glass surfaces in the epoxy-panels experience a lower strain than their silicone-panels counterparts – indicating the higher *DCA* of the former. Secondly, in transverse direction: the strain decay is more accentuated in the epoxy-panels than the silicone-panels – indicating the lower *EWR* of the former. Thirdly, in the longitudinal (span)-direction: in all tests the maximum strains were recorded at load locations rather than at mid-span (see Fig. 7).

The through-thickness strain distributions on the glass face-sheets are plotted in Appendix B (at a load $2{\cdot}P = 2$ kN). From the experimental distribution of strains and following the strain-based method reported by [12], the DCA_ε at each position is evaluated using Eq. 3.

$$DCA_\varepsilon = \frac{\varepsilon_{global}}{\varepsilon_{total}} \times 100\% \quad (3)$$

where ε_{total}, is the measured axial strain for each position, and ε_{global}, is found by first evaluating the average strain $\varepsilon_{average}$ between the outer and inner face sheet for each position as indicated in Fig. 8. Where $\varepsilon_{average} = 0$, compressive strains are equal to tensile strains but negative. Therefore, the average strains in the centre of the face sheet occur due to bending about the global axis. The average strain $\varepsilon_{average}$, is then extrapolated to the outer face sheet by a factor 34/24, following from the geometrical properties of the cross section to give ε_{global}.

The DCA_ε results were mirrored twice in-plane and visualised in a similar way as the strain maps, to obtain full DCA_ε maps as shown in Fig. 9. *DCA*s are plotted through-thickness for each experiment in a scale of 0–100 % where 0 % (white) refers to no composite action, and 100 % (black) infers full composite action.

4. Modelling and discussion

4.1. Effective width

The concepts of effective width, W_{eff}, and effective width ratio, *EWR*, derive from established research on the mechanical response behaviour of wide beams [6,7,9,10]. These concepts were first applied to 5-layer composite glazing panels by [1,26], according to Eqs. (4) and (5):

$$W_{eff} = 2 \bullet \int_0^{W/2} \frac{\epsilon(x)}{\epsilon_{\max}} dx \quad (4)$$

$$EWR = \frac{W_{eff}}{W} \quad (5)$$

(a)

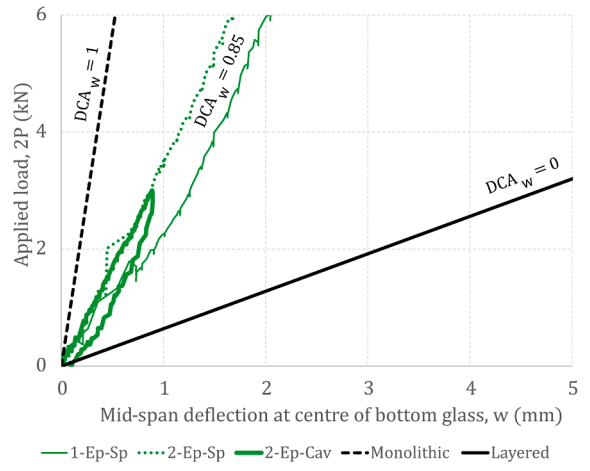

(b)

(c)

Fig. 6. Load-deflection responses at mid-span for (a) four experiments loaded to failure (config. Sp), and detailed views for (b) three experiments on Ep-panels (config. Sp & Cav) and (c) three experiments on Sil-panels (config. Sp & Cav). Note: $DCA_w = 0$, 1, and 0.85, are calculated in terms of mid-span deflections.

where x, is the coordinate across the width (Fig. 5a), ε, is the axial strain and ε_{max}, is its maximum value. In this paper, *EWR* values are calculated at the following locations: halfway into the shear span (*A* in Fig. 5a), at the full shear span (*B* in Fig. 5a) and halfway into the load span, corresponding to mid-span (*C* in Fig. 5a).

The results of *EWR* for each glass surface (top-outer, top-inner, bottom-inner and bottom-outer) are plotted in Fig. 10 (all panels) and are reported in Table 4 (Ep-panels) and Table 5 (Sil-panels), including cross-sectional and panel average values. The panel average values show $EWR = 0.90 \pm 0.02$ (Sil-panels) and $EWR = 0.68 \pm 0.04$ (Ep-panels) revealing more significant shear-lag effects on the epoxy-bonded panels. Overall, the shear-lag effects were more pronounced (i.e. lower *EWR*): (i) at loading locations (i.e. location *B*) than at mid-span (location *C*), and (ii) at the loaded face sheet (top) than at unloaded face sheet (bottom).

4.2. Deflection and strain prediction

The mechanical response (deflections and axial strains) was predicted by means of the analytical model developed by *Pascual et al.* for simply supported adhesively-bonded sandwich panels loaded in four-point bending [5]. The analytical solutions for strains and deflections are governed by the mechanical parameter α^2, given by Eq. 1 and are given by *Pascual et al.* [5]. This present study is relevant in that the width (*W*) used in the original model [5] for determining the flexural rigidities (*D*) is replaced by the average effective width (W_{eff}) from the average panel values reported in Table 4, Table 5 and Fig. 10. These average values, together with the resulting flexural rigidities and shear stiffnesses, are shown in Table 3.

The predicted responses and experimental results for the maximum deflections as measured by wire transducers fitted to the bottom glass face sheet (see Fig. 5a) are shown in Fig. 11. The predictions of the maximum deflection are in good agreement with the experimental results: discrepancies are within 15 %, except the double-edge spine silicone-bonded panel (*2-Sil-Cav*) where the analytically modelled solution overestimates the experimental result by 27 % at mid-span. This larger discrepancy may be explained by the fact that the prediction is based on a (multi-layer) beam-model, assuming constant deflection at every layer. However, the top glass of the tested panel *2-Sil-Cav* is loaded within the cavity area and therefore readily deflects. Meanwhile, due to low composite action, the bottom glass sheet is disconnected from the top glass sheet and therefore may deflect less. An average value of deflections as measured at the top and bottom face sheet may show closer agreement with the predictions of the model.

The predicted responses and experimental results for the maximum strains as measured by strain gauges (see Fig. 5a) are shown in Fig. 12. The prediction of strains was accurate at mid-span (cross-section *C*), with less than 16 % difference between the analytical solutions and experimental data. Larger differences were observed at the loaded cross-section, especially for panels loaded in config. *Cav*. This discrepancy is attributed to high stress/strain concentrations near the loading points (i.e. cross-section *B* – see Fig. 5), which were not adequately captured by the analytical model and is a known limitation of effective width methods in the analysis of shear-lag.

4.3. Discussion

For epoxy-bonded panels, the Euler-Bernoulli simple beam theory (i.e. fully monolithic behaviour: no shear distortion of adhesive and *EWR* = 1) leads to a 67 % underestimation of maximum deflections and 50 % underestimation of strains, see Figs. 11b and 12b. This illustrates the need for a more detailed model, e.g. such as the model by *Pascual et al.* with realistic values of *EWR*, for a safe and efficient prediction of the mechanical response [5].

On the other hand, for silicone-bonded panels, the simplified

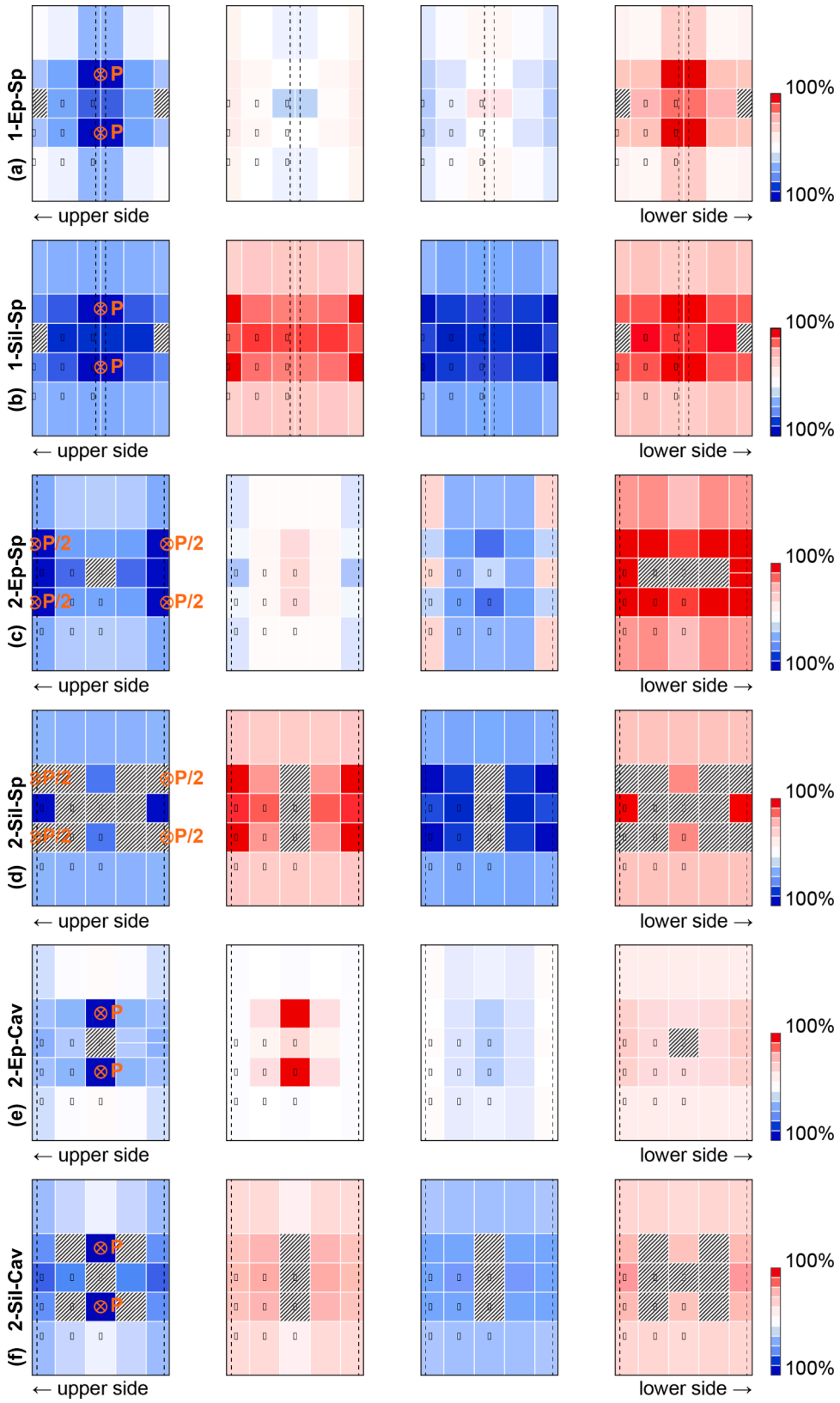

Fig. 7. Normalised maps of experimental longitudinal strains at $2{\cdot}P = 2$ kN for (a-b) single-spine panels in config. *Sp.*, (c-d) double-spine panels in config. *Sp*, and (e-f) double-spine panels in config. *Cav*. Note: blue (compression), red (tension), grey (dysfunctional gauges).

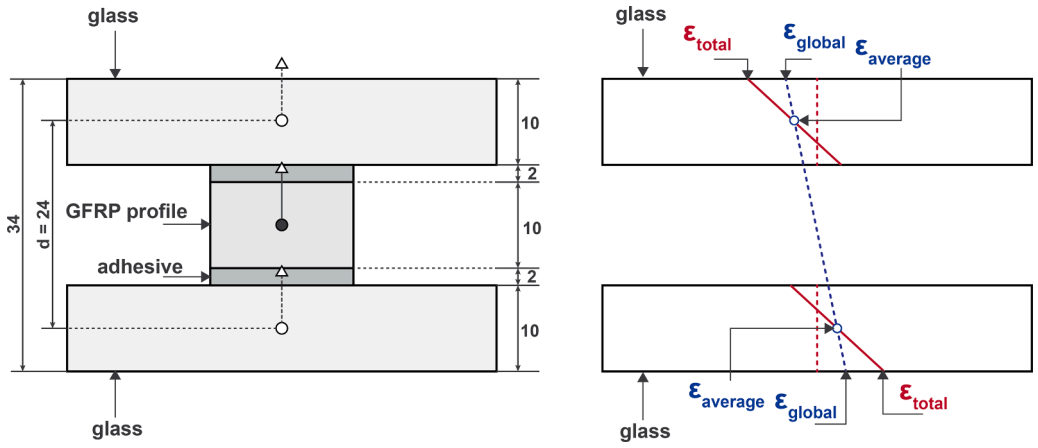

Fig. 8. Through thickness geometrical properties of composite glazing panels and longitudinal strain distribution in glass panes (shown for cross-section of central spine panel). Measurements shown in mm.

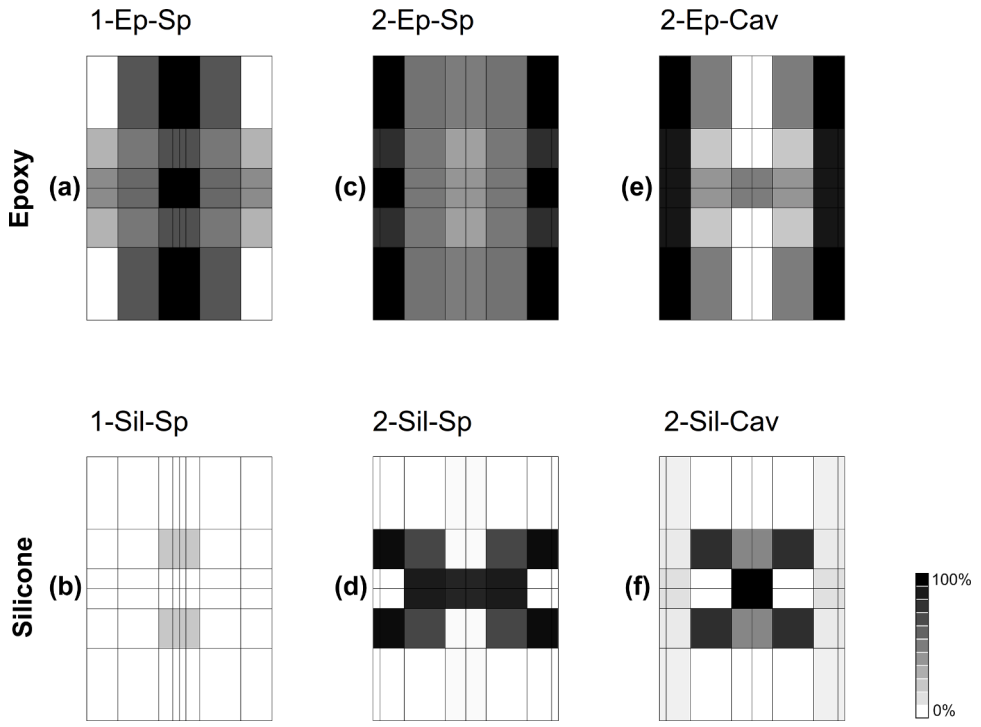

Fig. 9. DCA_e maps for (a-b) single-spine panels in config. *Sp*. (c-d) double-spine panels in config. *Sp*, and (e-f) double-spine panels in config. *Cav*. Note: DCA_e calculated in terms of strain distributions (strain distributions shown in Appendix B).

assumption of layered behaviour (i.e. no shear connection between layers and $EWR = 1$) produces a reasonably good prediction of deflections and strains, see Figs. 11a and 12a. In this case, the benefits of using a more sophisticated model are marginal.

However, from a material efficiency perspective, it is evident that silicone-panels are mechanically inefficient and underperform compared to epoxy panels in terms of mid-span deflections (400 % larger), mid-span strains/stresses (200 % greater), and maximum load capacities (up to 35 % smaller), see Table 1 and Figs. 11 and 12. This inefficiency results from the shear compliance of silicone bonds compared to the stiffer epoxy bonds – the former always produces low *DCA*s whilst the latter still allows for relatively high *DCA*s, particularly at close-to-spine regions, see Fig. 7. Mechanically, this translates into layered behaviour (local bending) prevailing in silicone panels and monolithic behaviour (global bending) prevailing in close-to-spine regions of epoxy panels, see Fig. 13. As shown in Fig. 14 and Appendix B, on close inspection of the strain states, it is evident that layered behaviour dominates in the far-from-spine regions of the epoxy-bonded panels.

5. Conclusions

Composite glazing panels, consisting of glass face sheets adhesively bonded to linear stiffeners (spines) in the core region, were assembled

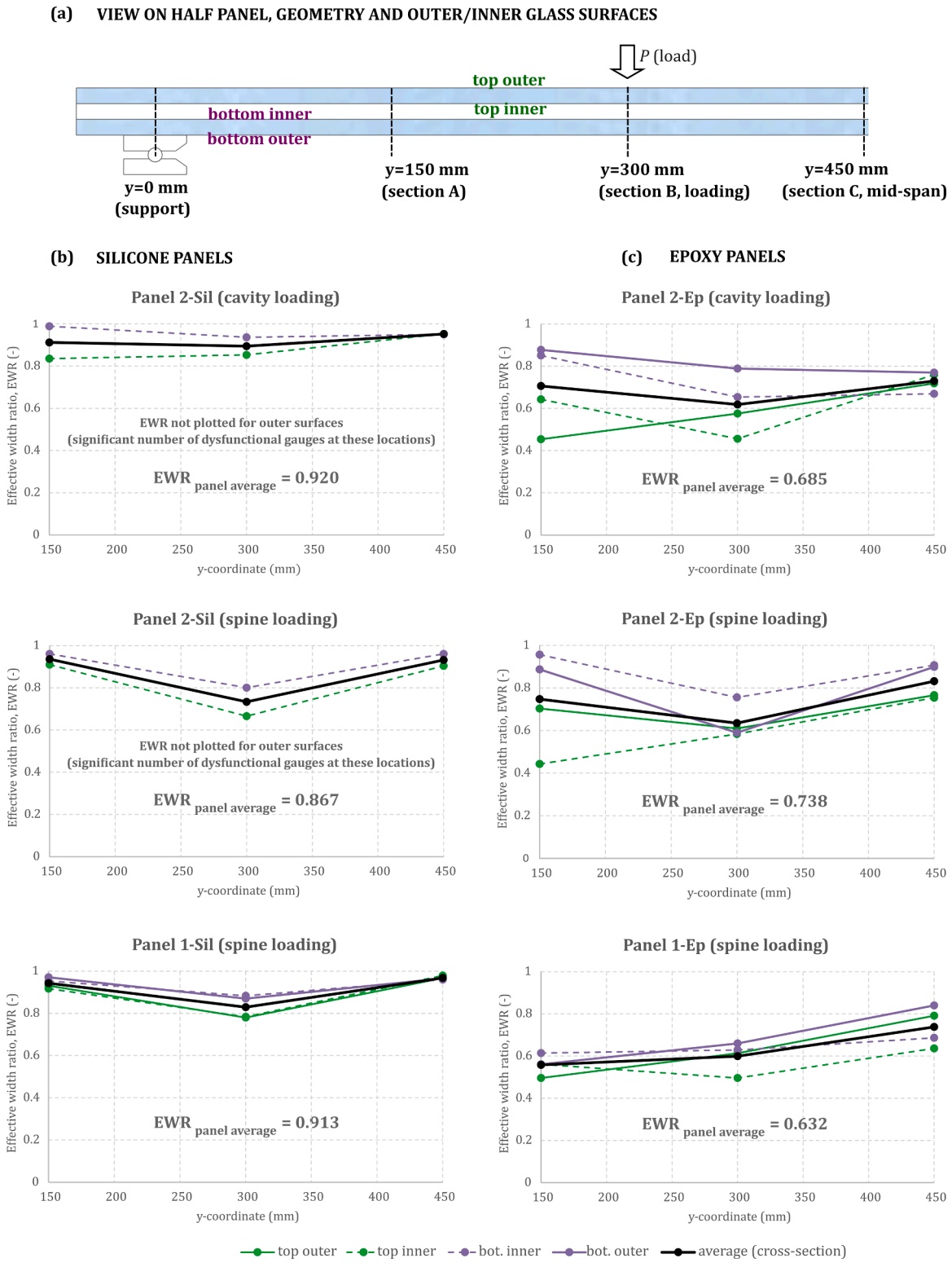

Fig. 10. Experimental results on effective widths showing (a) geometry and labelling of inner/outer glass surfaces, (b) *EWR* for silicone panels on inner/outer glass surfaces and (c) *EWR* for epoxy panels on inner/outer glass surfaces.

Table 4
Effective width ratio (*EWR*) for epoxy panels at locations *A*, *B* and *C* and average values for cross-section and whole panel.

Location	Panel 2-Ep (*Cav* loading)			Panel 2-Ep (*Sp* loading)			Panel 1-Ep (*Sp* loading)		
Face-sheets	*EWR*, at locations *A* to *C*			*EWR*, at locations *A* to *C*			*EWR*, at locations *A* to *C*		
Glass surface	*A*	*B*	*C*	*A*	*B*	*C*	*A*	*B*	*C*
Top-outer	0.454	0.576	0.719	0.703	0.610	0.766	0.496	0.613	0.791
Top-inner	0.643	0.456	0.760	0.443	0.584	0.754	0.561	0.496	0.636
Bot-inner	0.851	0.654	0.669	0.956	0.756	0.907	0.614	0.629	0.686
Bot-outer	0.877	0.789	0.770	0.887	0.590	0.899	0.561	0.660	0.840
Avg. (cross-sec.)	0.706	0.619	0.729	0.747	0.635	0.831	0.558	0.599	0.738
Avg. (panel)	0.685			0.738			0.632		

Table 5
Effective width ratio (*EWR*) for silicone panels at locations *A*, *B* and *C* and average values for cross-section and whole panel. Note: Values marked with (*) were excluded for average calculations as a significant number of strain gauges were dysfunctional at these locations.

Location	Panel 2-Sil (*Cav* loading)			Panel 2-Sil (*Sp* loading)			Panel 1-Sil (*Sp* loading)		
Face-sheets	*EWR*, at cross-sections *A* to *C*			*EWR*, at cross-sections *A* to *C*			*EWR*, at cross-sections *A* to *C*		
Glass surface	*A*	*B*	*C*	*A*	*B*	*C*	*A*	*B*	*C*
Top-outer	*0.626**	*0.599**	*0.791**	*0.991**	*0.540**	*0.673**	0.931	0.780	0.967
Top-inner	0.836	0.853	0.953	0.910	0.666	0.904	0.917	0.784	0.979
Bot-inner	0.989	0.937	0.951	0.961	0.801	0.961	0.953	0.883	0.960
Bot-outer	*0.916**	*0.820**	*0.844**	*0.923**	*0.923**	*0.840**	0.971	0.870	0.966
Avg. (cross-sec.)	0.912	0.895	0.952	0.936	0.734	0.933	0.943	0.829	0.968
Avg. (panel)	0.920			0.867			0.913		

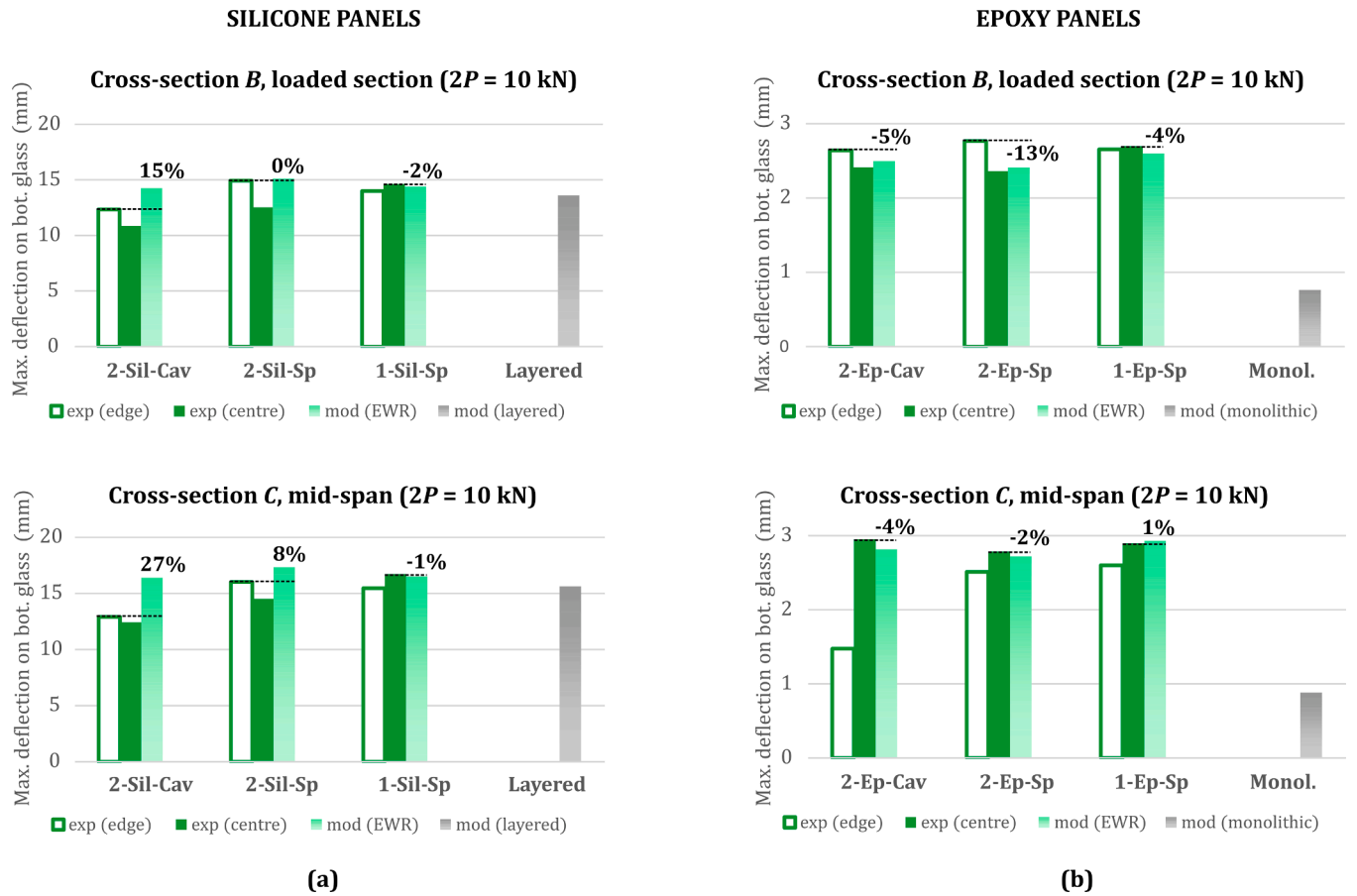

Fig. 11. Experimental and modelled deflections of bottom glass face-sheet (on edge & central position) at $2{\cdot}P = 10$ kN for (a) silicone panels and (b) epoxy-panels. The percentage values shown above the modelled deflection plot denote the level of agreement between the analytically modelled results and the experimental data, where the largest value from the experimental data was taken as reference. *Note: experimental data for panels 2-Sil and 2-Ep extrapolated linearly from values at $2{\cdot}P = 2$ kN.

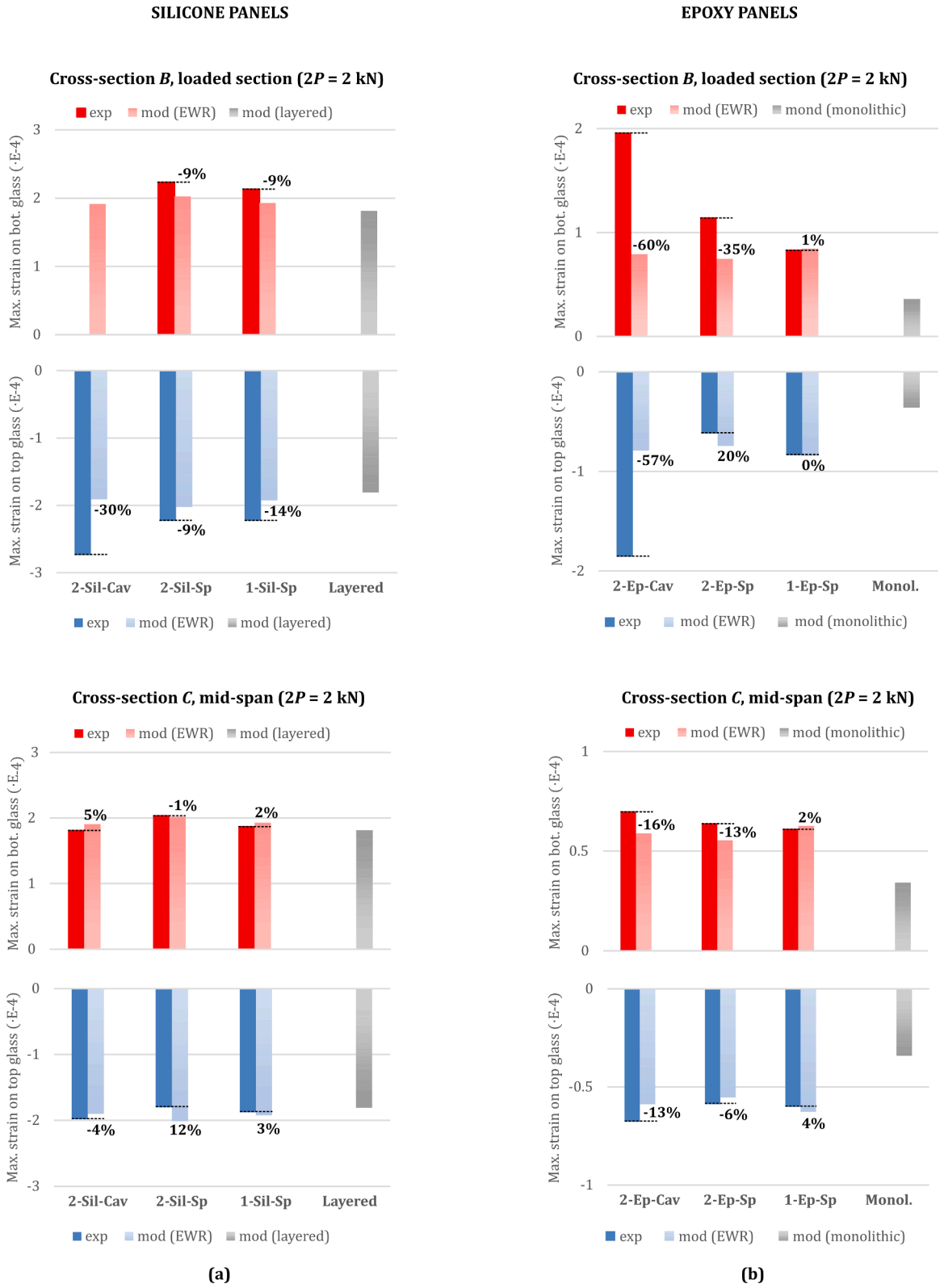

Fig. 12. Experimental and modelled maximum axial strains on glass face-sheets at $2{\cdot}P = 2$ kN for (a) silicone panels and (b) epoxy-panels. The percentage values shown above the modelled strain plot denote the level of agreement between the analytically modelled results and the experimental data. Note: no reliable data was recorded at cross-section B on the bottom glass of 2-Sil-Cav due to dysfunctional gauges.

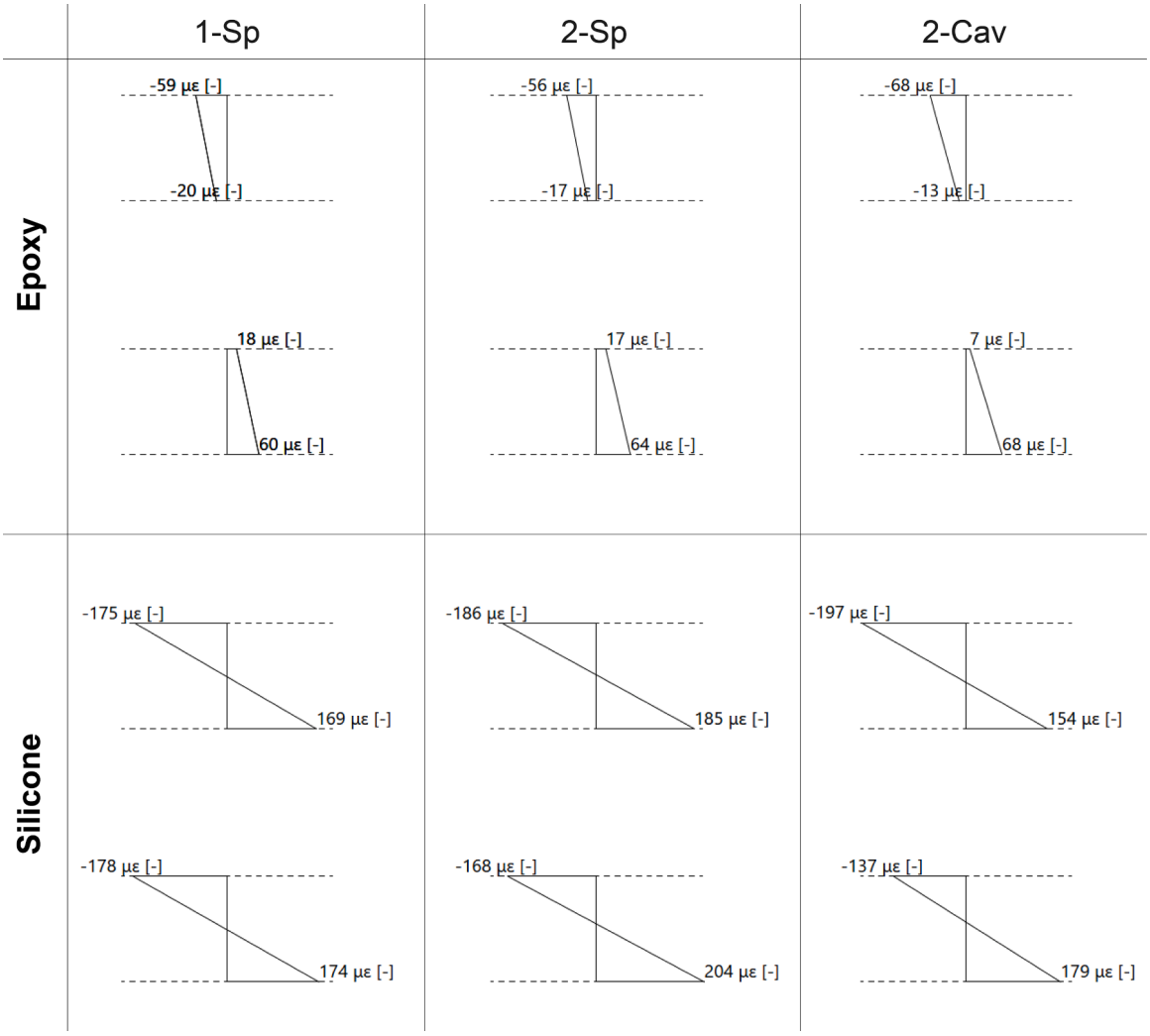

Fig. 13. Through-thickness strain distribution at mid-span (position C1 close-to-spine, see Fig. 5) for silicone-bonded panels and epoxy-bonded panels obtained from experimental data. The small differences in absolute strain values between the top and bottom face sheets are attributed to experimental error.

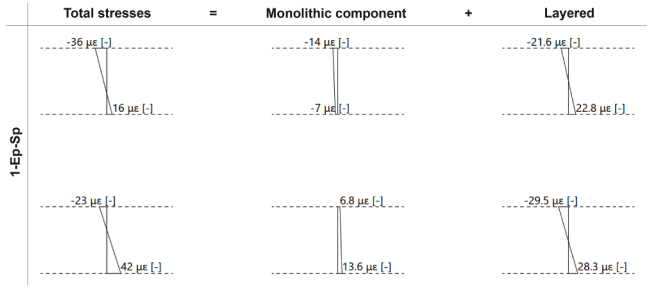

Fig. 14. Through thickness strain distribution at mid-span (position C3 far-from-spine, see Fig. 5) obtained from experimental data and decomposed into monolithic and layered components for epoxy panel 1-Ep-Sp. The small differences in absolute strain values between the top and bottom face sheets are attributed to experimental error.

and tested in a four-point bending configuration. Panels with different adhesives (epoxy and silicone) were tested with different spine locations (central and edge) and different load locations (on-spine and on-cavity), primarily to investigate shear-lag effects in 5-layer composite glazing panels. It was found that:

1. Shear-lag effects are more significant in the epoxy-bonded panels than in the silicone-bonded panels. Overall, the face-sheets of epoxy and silicone-bonded panels exhibited average effective width ratios ($EWR_{average}$) of 0.68 ± 0.04 and 0.90 ± 0.02 respectively.
2. The degree of composite action, in terms of mid-span deflections, of epoxy and silicone-bonded panels were approximately equal to 0.85 and 0, respectively.
3. The model by *Pascual et al.* [5], with *EWR* values obtained from this study produced predictions of maximum strains at mid-span within 16 % of the experimental results. However, strain concentrations at load application points were not always captured accurately.
4. The assumption of monolithic behaviour for composite panels with stiff adhesives (e.g. epoxy-bonded panels in this study) leads to significant underestimations of deflections and strains (up to 67 % in this study) and is therefore unsafe. Conversely, the assumption of a layered behaviour for flexible adhesives (e.g. silicone-bonded panels in this study) is sufficiently accurate.
5. Epoxy-bonded panels outperform silicone panels in terms of stiffness and strength. For the design and analysis of these panels, the model by *Pascual et al.* and the *EWR* results of this research constitute valuable tools for predicting their mechanical performance [5].

Future work should focus on the limits of applicability of *EWR* values for real-world engineering design applications. This should include an

investigation into the absolute limits of the effective width for panels with very widely spaced spine cores; such a limit is expected due to significant shear-lag effects at large distances from the spines and from geometric instability (i.e. buckling) of compressed slender face-sheets at these far-from-spine locations. A numerical parametric study using finite element analyses on composite glazing panels would further support this. This study sought to demonstrate shear-lag effects in composite glazing panels at the upper and lower bound of performance in terms of *DCA*. Future work would benefit from investigations into the significance of shear-lag effects in the presence of adhesives that exhibit intermediate stiffness, such as polyurethanes. The consideration of other non-linearities (e.g. adhesive mechanical response in shear as shown in Appendix A) also merit further research to address the linear elastic assumptions of this work. In addition, research on the prediction of ultimate loads (strength) is required to better understand the mechanical performance of composite glazing panels.

Furthermore, polymeric adhesive connections in the AEC sector are currently designed for long-term durability with few considerations for disassembly. Future work is required to develop ways of separating the components of composite glazing units (e.g. glass and structural profiles) from one another in a safe and efficient manner to enable reuse and recycling at end of life.

CRediT authorship contribution statement

Carlos Pascual: Writing – review & editing, Writing – original draft, Visualization, Validation, Methodology, Investigation, Funding acquisition, Formal analysis, Data curation, Conceptualization. **Rebecca Hartwell:** Writing – review & editing, Writing – original draft, Visualization, Methodology, Investigation, Data curation. **Pim Buskermolen:** Writing – review & editing, Writing – original draft, Visualization, Validation, Methodology, Formal analysis. **Mauro Overend:** Writing – review & editing, Writing – original draft, Supervision, Methodology, Funding acquisition, Conceptualization.

Declaration of Competing Interest

The authors declare the following financial interests/personal relationships which may be considered as potential competing interests, Carlos Pascual reports financial support was provided by Engineering and Physical Sciences Research Council. Rebecca Hartwell reports financial support was provided by Engineering and Physical Sciences Research Council. Carlos Pascual reports financial support was provided by Ove Arup and Partners. If there are other authors, they declare that they have no known competing financial interests or personal relationships that could have appeared to influence the work reported in this paper.

Acknowledgements

This research was part-funded by the UK Engineering and Physical Sciences Research Council through EPSRC IAA Follow-on Fund, the Centre for Doctoral Training in Future Infrastructure and Built Environment (EPSRC grant reference number EP/L016095/1), and Ove Arup & Partners (London). The authors are grateful to Peter Lenk (formerly of Ove Arup & Partners, London) for discussions on the mechanics of shear-lag, and to Cambridge University Structures Laboratory (United Kingdom) for the support in the experimental campaign. The authors also acknowledge the in-kind contributions of Interpane (glass), Fiberline Composites (GFRP profiles), Dow (silicone adhesive) and H.B. Fuller-Koemmerling (epoxy adhesive).

Appendix A: Characterization of adhesive joints

Six single-lap shear specimens were fabricated using epoxy adhesive EP40619 (three specimens) and silicone adhesive Dow 121 (three specimens) with two lap joints per specimen. In each specimen the substrates consisted of two 50-mm wide by 10-mm thick by 190-mm long GFRP bars and a 200 × 150 x 10 mm fully toughened glass plate. The GFRP bars were milled down by about 0.1-mm, using an electric sanding device, to remove their resin-rich surface layer. The bonded areas A, were 50 × 20 mm for every lap joint and adhesive layers were 2-mm thick ($h_{adh} = 2$ mm). To ensure the correct alignment of GFRP and glass components, and also a constant thickness of adhesive layers, the specimens were produced using bespoke polytetrafluorethylene moulds (see Fig. A1). The specimens were cured at 23 ± 2°C for a minimum of seven days before testing. The specimens were pin-ended and connected to a 30-kN electromechanical testing machine (Instron 5567), see Fig A1. The tests were performed up to failure at low displacement rates of 1 mm/min (silicone joints) and 0.2 mm/min (epoxy joints) and at laboratory conditions of 23 ± 2 °C and 50 ± 10 % relative humidity. Two sets of data were recorded: 1) the tensile loading force, F, applied by the machine, and 2) the relative displacements, Δl, between glass and GFRP as measured by two laser extensometers (one per lap joint), see Fig. A1. The times to failure were approximately 800–1300 s (silicone joints) and 1000–1500 s (epoxy joints). The failure of the joints can be classified, according to ASTM D5573–99 [27] as: adhesive failure (epoxy specimens 1 and 2) and fibre-tear failure (epoxy specimen 3), and cohesive failure (all silicone specimens), see Fig. A1.

The F-Δl curves are shown in Fig. A2 for the two lap joints per specimen. The responses were slightly non-linear (silicone joints) and highly non-linear (epoxy joints) and showed a progressive decrease of stiffness with increasing tensile load. The shear strength (at failure) and initial elastic and shear moduli (at about 10 % of the strength) were calculated for a constant shear stress (F/A) and shear distortion ($\Delta l/h_{adh}$) over the bonded areas and are reported in Table A1. The mismatches of initial elastic and shear moduli calculated here compared to the values obtained from hardness data given by manufacturers, and used above for the predictions of strains and deflections, were only of about 10 % (epoxy) and 0 % (silicone), Table A1 and Table 2.

It is to be noted that the non-linear response of single-lap shear specimens (Fig. A2) contrasts with the linear response of the panels tested in bending (Fig. 6). The linear response of the panels may be due to the confinement of the adhesives (due to the significant length of the adhesive bonds along the spines) preventing therefore the development of notable plastifications and maintaining the adhesives in their initial linear elastic responses with higher stiffness. However this hypothesis requires further investigation.

Table A1
Shear strength, initial elastic modulus and initial shear modulus of adhesives based on the results of single-lap shear experiments. *Note: mismatch with elastic properties reported in Table 2 (calculated from hardness data given by manufacturer)

Lap joint	Shear strength	Elastic properties		
Adhesive bond	τ (MPa)	E (MPa)	G (MPa)	Δ*
Epoxy EP40619	8.96 ± 0.57	342.6 ± 48.6	123.2 ± 17.5	−10 %
Silicone Dow 121	1.04 ± 0.07	1.49 ± 0.09	0.50 ± 0.03	0 %

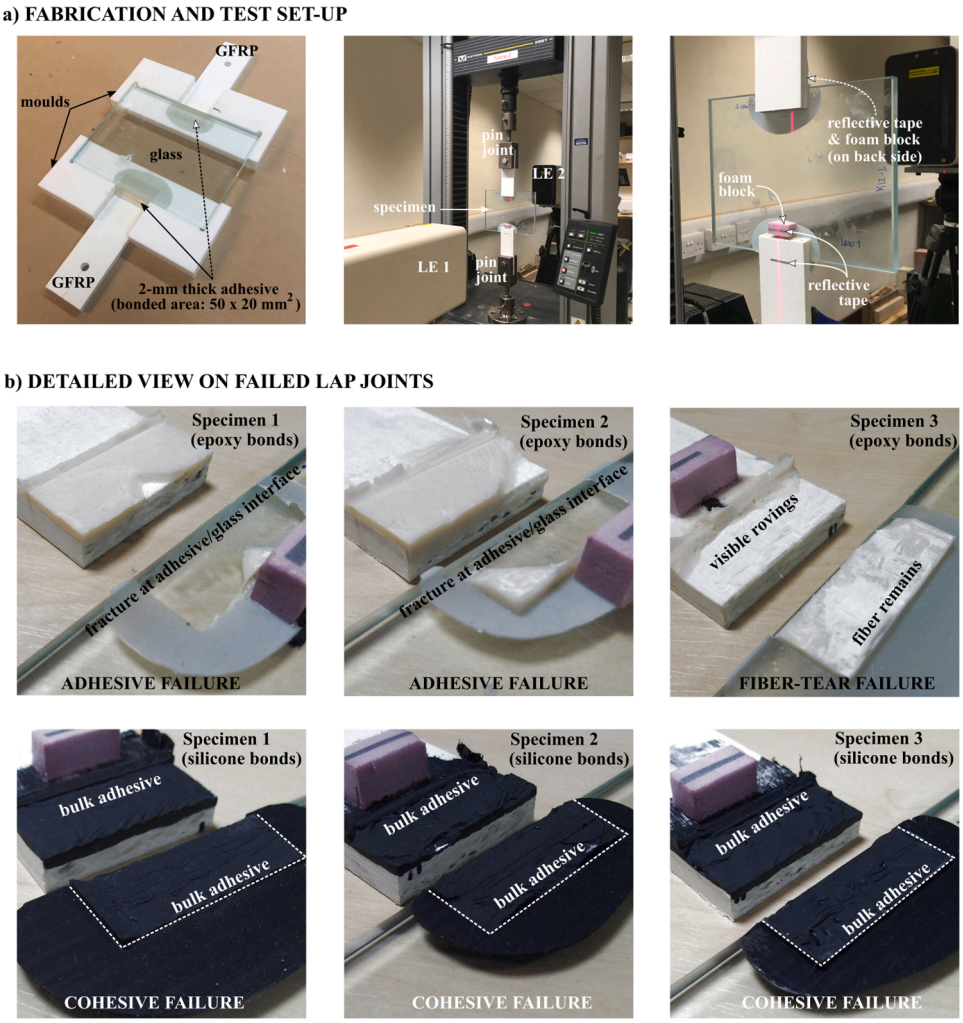

Figure A1. Views on (a) polytetrafluorethylene moulds for single-lap shear specimen fabrication and test set-up showing a 30-kN electromechanical testing machine and two measuring laser extensometers (LE) and (b) failed lap joints of epoxy and silicone specimens

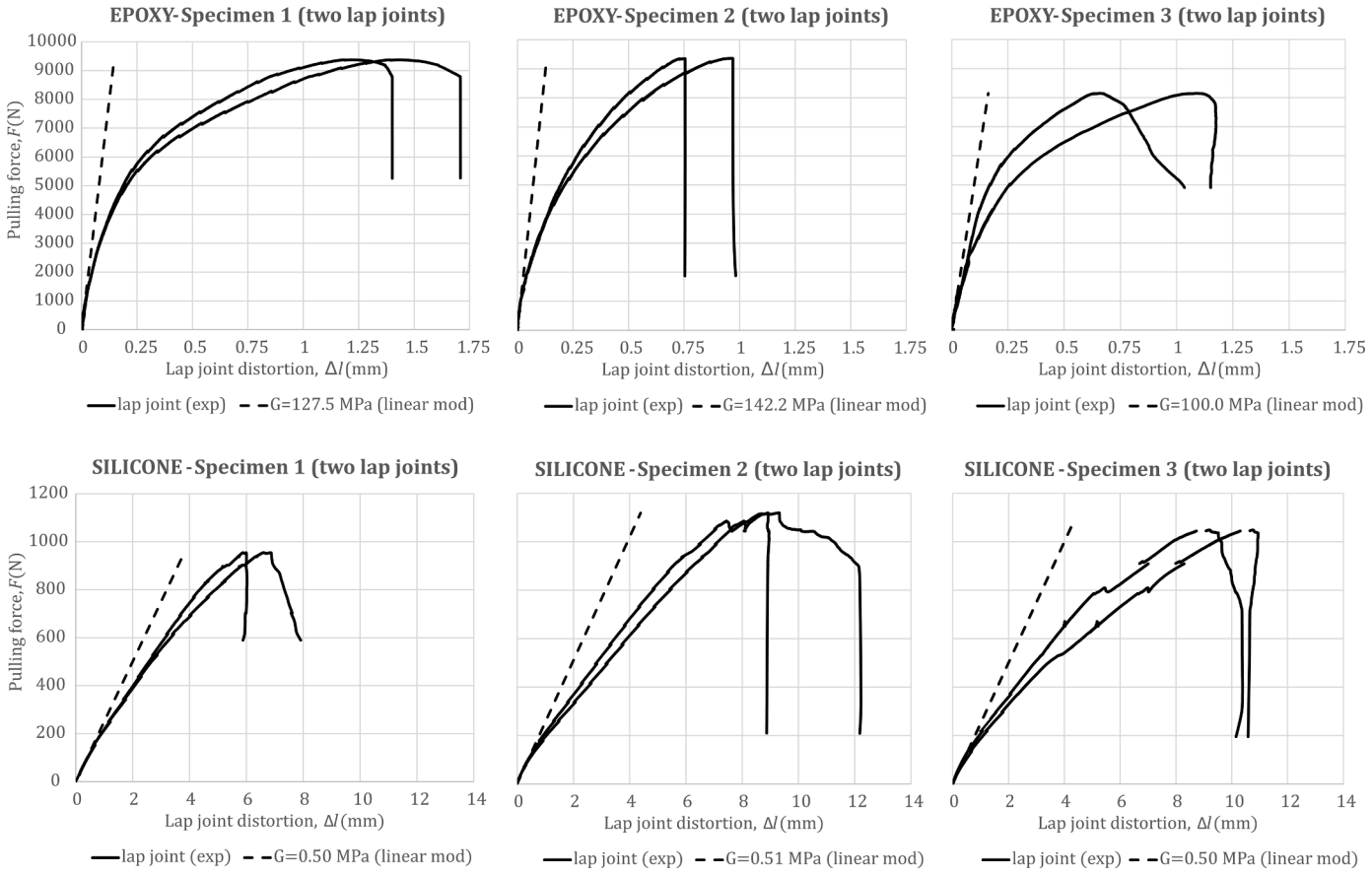

Figure A2. Experimental load-displacement response of epoxy-bonded (3 specimens) and silicone-bonded (3 specimens) single-lap shear joints together with modelled linear response based on initial stiffness. Note: two lap joints per specimen

Appendix B: Cross-sectional strain plots at $2{\cdot}P = 2$ kN

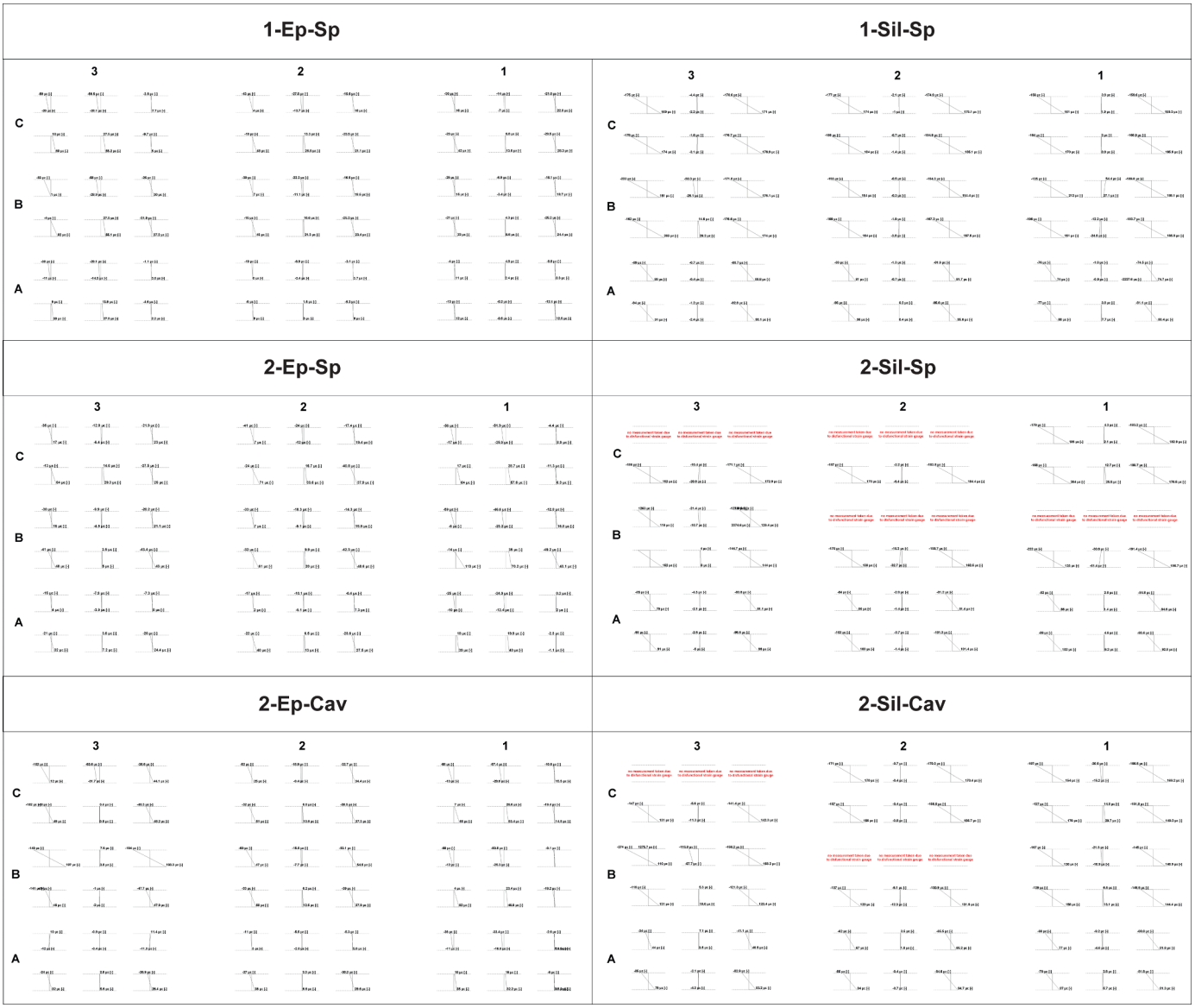

Figure B1. Through-thickness strain distribution at every *(x-y)* gauge location (see Figure 4) decomposed in local (layered) and global (monolithic) components

Data availability

Data will be made available on request.

References

[1] Pascual C, Nhamoinesu S, Overend M. The flexural response of large scale steel-framed composite glazing panels. Glass Struct Eng 2019.
[2] Pascual C, Overend M. Buckling of sandwich struts with a particular application in composite multi-layer glazing. Eng Struct 2021:230.
[3] Heinisuo M, Pajunen S. CLT beam analysis using classical elastic theory of layered beams. Raken Mek 2021;54(4):143–71.
[4] Chen A, Bazroun M, Yossef M. Analysis of multi-layers insulated sandwich panel with flexible shear connectors. Mech Adv Mater Struct 2022;29(28):7375–86.
[5] Pascual C, Montali J, Overend M. Adhesively-bonded GFRP-glass sandwich components for structurally efficient glazing applications (Available from) Compos Struct [Internet] 2017;160:560–73. https://doi.org/10.1016/j.compstruct.2016.10.059.
[6] Girkmann K. Flächentragwerke. Springe Berl Heidelb 1959.
[7] Moffat KR, Dowling PJ. Shear lag in steel box girder bridges. Struct Eng 1975;53(10):439–48.
[8] Kristek V, Skaloud M. Advanced Analysis and Design of Plated Structures. Elsevier Science Ltd; 1991.
[9] Reissner E. Analysis of shear lag in box beams by the principle of minimum potential energy. Q Appl Math 1946;4:268–78.
[10] Reissner E. Least work solutions of shear lag problems. J Aeronaut Sci 1941;8.
[11] Yossef M, Chen A. Effective width of insulated sandwich panels with interior flexible frp shear connectors considering partial degree of composite action 2017;143(9):1–6.
[12] Yossef M, Chen A. A solution considering partial degree of composite action for insulated sandwich panels with general con fi guration fl exible shear connectors. Eng Struct 2018;162(January):135–50.
[13] CEN. EN 13706-3: 2002: Reinforced plastics composites. Specifications for pultruded profiles. Specific requirements. British Standards Institution; 2002.
[14] CEN. EN 572-2:2012: Glass in building. Basic soda lime silicate glass products Float glass. British Standards Institution; 2012.
[15] CEN. EN 12150-2:2004: Glass in building. Thermally toughened soda lime silicate safety glass - Evaluation of conformity/Product standard. 2004.
[16] Overend M, Jin Q, Watson J. The selection and performance of adhesives for a steel – glass connection (Available from:) Int J Adhes Adhes [Internet] 2011;31(7):587–97. https://doi.org/10.1016/j.ijadhadh.2011.06.001.

[17] Belis JLIF, Hulle van A, Out B, Bos FP, Callewaert D, Poulis H. Broad screening of adhesives for glass-metal bonds. Proc Glass Perform Days 2011:286–9.
[18] Nhamoinesu S, Overend M. The Mechanical Performance of Adhesives for a Steel-Glass Composite Façade System (Delft) Challenging Glass 2012;3:293–306.
[19] Fiberline Composites A/S. Fiberline Design Manual [Internet]. 2003. Available from: https://fiberline.com/design-manual
[20] Haldimann M, Luible A, Overend M. Structural use of glass. Zurich: International Association for Bridge and Structural Engineering; 2008.
[21] CEN. EN 572-1:2012: Glass in building - Basic soda lime silicate glass products - Part 1: Definitions and general physical and mechanical properties. British Standards Institution; 2012.
[22] Larson K. Can You Estimate Modulus From Durometer Hardness for Silicones? Yes, but only roughly … and you must choose your modulus carefully!. Dow Corning Corporation; 2017.
[23] Qi HJ, Joyce K, Boyce MC. Durometer hardness and the stress-strain behaviour of elastomeric materials. Rubber Chem Technol 2003:419–35.
[24] Haldimann M, Luible A, Overend M. Structural use of glass. Zurich: International Association for Bridge and Structural Engineering; 2008.
[25] Vandebroek M, Louter C, Caspeele R, Ensslen F, Belis J. Size effect model for the edge strength of glass with cut and ground edge finishing. Eng Struct 2014;79:96–105.
[26] Nhamoinesu S. Steel-glass composite panels. Univ Camb 2015.
[27] ASTM. ASTM D5573-99. Standard Practice for Classifying Failure Modes in Fiber-Reinforced-Plastic (FRP) Joints. American Society for Testing and Materials; 2012.